H-Atom Assignment and Sb–O Bonding of [Mes_3SbOH][O_3SPh] Confirmed by Neutron Diffraction, Multipole Modeling, and Hirshfeld Atom Refinement

John S. Wenger,[a] Xiaoping Wang,[b] and Timothy C. Johnstone[a]*

[a] Department of Chemistry and Biochemistry, University of California Santa Cruz, Santa Cruz, California 95064, United States.

[b] Neutron Scattering Division, Oak Ridge National Laboratory, Oak Ridge, Tennessee 37831, United States.

KEYWORDS. Neutron diffraction, charge density, AIM, multipole model, Hirshfeld atom refinement, stibonium

ABSTRACT Neutron wavelength-resolved Laue diffraction experiments permit accurate refinement of the H-atom positions and anisotropic displacement parameters of [Mes_3SbOH][O_3SPh]. A multipole-based charge density refinement and a topological analysis of the refined electron density were also performed. Hirshfeld atom refinement (HAR) recovers the neutron-determined H-atom parameters and the quantum-mechanical electron density used in HAR recovers the electron density topology from the refined multipole model. These results confirm that [Mes_3SbOH][O_3SPh] does indeed feature a hydroxystibonium cation with a nominal Sb–O single bond and not a stibine oxide with a Sb=O/Sb^+–O^- bond.

A recent investigation into the chemistry of stibine oxides uncovered only two well-characterized examples of putative monomeric stibine oxides: $Mes_3SbO\cdots HO_3SR$, where R = Ph and CF_3.[1-2] Our reanalysis of these substances revealed, however, that both in fact feature the hydroxytrimesitylstibonium cation. Although we used a variety of orthogonal techniques to support this conclusion, our selection of the $[Mes_3SbOH][O_3SR]$ formulation over $Mes_3SbO\cdots HO_3SR$ rested most heavily on the complication-fraught location of an H atom in an independent atom model (IAM) X-ray crystal structure.

During our investigation of the $[Mes_3SbOH][O_3SR]$ compounds, a new implementation of Hirshfeld atom refinement (HAR), *NoSpherA2* (non-spherical atom refinement in *Olex2*),[3] was released.[4] *NoSpherA2* builds upon a decade of successful development in the area of HAR,[5-10] in which the electron density of the model is obtained from DFT calculations and is used to produce aspherical atomic form factors for further refinement. HAR belongs to the field of quantum crystallography, in which quantum mechanically calculated wavefunctions are used to simulate the electron density of the model and obtain the calculated structure factors.[11-14] Validation studies have demonstrated that HAR of H-atom positions and anisotropic displacement parameters (ADPs) returns values comparable to those obtained from neutron diffraction.[7-8,15]

Herein, we describe refinement of the neutron crystal structure of $[Mes_3SbOH][O_3SPh]$ and confirm that HAR is able to fully recover the H-atom positions in this H-bonded, heavy-atom structure. Using the neutron-refined H-atom parameters, we performed a multipole-model (MM) charge density refinement against the X-ray structure factors. We conducted parallel topological analyses on the MM and HAR electron densities and demonstrate that topological analysis of the electron density provided by the ORCA software during the *NoSpherA2* routine affords the same results as such an analysis of the refined MM charge density.

A single-crystal wavelength-resolved Laue neutron diffraction experiment was performed on a prism of [Mes_3SbOH][O_3SPh] measuring 1.08 × 0.80 × 0.35 mm^3 using TOPAZ at the Spallation Neutron Source of Oak Ridge National Laboratory. Because of the large number of H atoms, the positions and ADPs of non-H atoms were constrained to the values from our previously published X-ray IAM; H-atom positions and ADPs were freely refined. The neutron data revealed the presence of disorder in one of the methyl groups that had gone undetected in the IAM X-ray refinement (Figure 1A). The H atom between SbO and OS is clearly visible (SbO–H = 0.98(2) Å) and provides definitive confirmation of our earlier assignment of this species as a hydroxystibonium salt. The observed X–H bond lengths across the entire structure (Table S2) agree well with averaged neutron diffraction data (Table S3).[16]

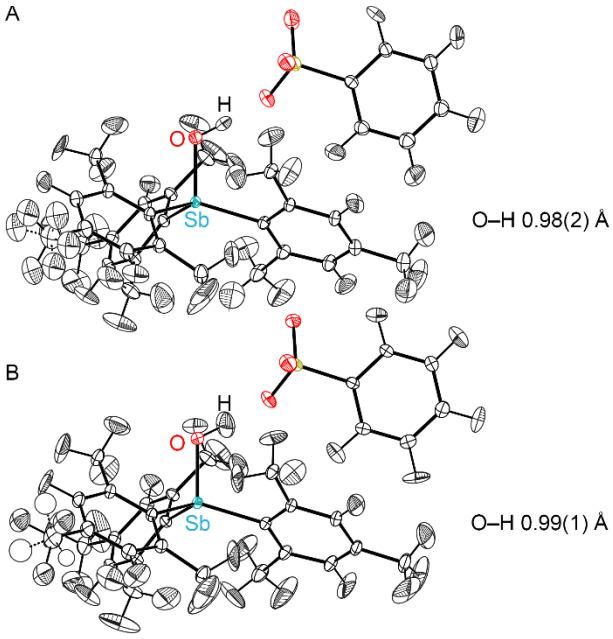

Figure 1. Thermal ellipsoid plots (50% probability level) of [Mes_3SbOH][O_3SPh] from the (A) neutron diffraction and (B) X-ray diffraction (HAR) crystal structures. In (B), the H atoms in the minor component of the disorder, which are refined with isotropic thermal parameters, are shown as spheres. Color code: Sb teal, O red, S yellow, C black, H grey.

Neutron diffraction provides powerful insight into such systems, but we appreciate that it is not always possible for researchers to access this analytical method. Moreover, neutron diffraction typically requires larger crystals than X-ray diffraction and single crystals of sufficiently high quality can be very difficult to obtain. Encouraged by developments in the description of H-atoms using HAR,[7-8,15] and the flexibility in refinement options and theoretical model chemistries offered through *NoSpherA2*,[4] we performed a Hirshfeld atom refinement of [Mes_3SbOH][O_3SPh] (details in SI). The PBE0-DKH2/x2c-TZVPP[17-19] electron density at the IAM coordinates was used to obtain aspherical atomic form factors, which were used for a new round of least-squares refinement of the model. The model chemistry for the quantum chemical calculations was selected to provide a balance of accuracy and speed while accounting for the relativistic effects of the heavy Sb atom. The newly refined atomic coordinates were used as the input for a new DFT calculation, from which new aspherical form factors were obtained. This procedure was iterated until it had converged.

In the resulting intermediate HAR model (data not shown), the H-atom displacement ellipsoids were well-formed with the exception of a single methyl group. This methyl group is the same that was observed to be disordered in the neutron diffraction data, highlighting that HAR can allow H-atom disorder to be discerned from X-ray data in instances where it is not even evident in X-ray IAM refinement. In our final HAR model (Figure 1B, Table S1), the methyl disorder was included with similarity and rigid-bond restraints and the minor component was refined using isotropic H-atom thermal parameters. The C–H bond lengths from the neutron structure and the HAR structure exhibit a RMSD of only 0.036 Å. The ADPs from the two models also agree well with an average correlation coefficient of 0.84 (Figure S1, Table S7).[20] This agreement

adds to the evidence highlighting that HAR analysis of home-source X-ray data can afford neutron-quality H-atom parameters even for crystals with heavy atoms and intermolecular H-bonding.[4]

Using our X-ray data set and the accurate, neutron-refined H-atom positions and ADPs, we performed a multipole refinement of $[Mes_3SbOH][O_3SPh]$ using the Hansen-Coppens formalism (details in SI). In contrast to the difference Fourier synthesis of the IAM structure, which shows extensive residual electron density on bonds and at lone pairs (Figure S2), the corresponding difference Fourier maps of the MM are much less featured (Figure S3). We do note that there is unsurprisingly residual electron density proximal to the heavy Sb atom, highlighting that caution should be exercised in interpreting these results because of the possible influence of extinction effects or anharmonic thermal motion, which have not been refined in the present model.

A search of the MM electron density (ρ) for topologically critical points (Figure 2) revealed (3, –3) critical points at the locations of all nuclei and (3, –1) critical points (bond critical points, BCPs) between all pairs of covalently bonded atoms. As expected, the value of ρ at a BCP (ρ_b) is greater for the C_{Ar}–C_{Ar} than the C_{Ar}–C_{Me} bonds of the mesityl rings (Figure 3, Table S8).[21] The values of the Laplacian of the electron density for all of the BCPs ($\nabla^2\rho_b$) associated with the covalent C–C, C–H, S–O, and S–C bonds were < 0, as expected (Figure 3, Table S8). The Sb–O and Sb–C bonds featured positive $\nabla^2\rho_b$ values, as has been previously reported for polar covalent bonds involving heavy atoms.[22] The MM also featured a BCP between H1 (Sb–O*H*) and O2 (S*O*) (Figure 2). The low ρ_b (0.053 e^- $bohr^{-3}$) and positive $\nabla^2\rho_b$ (0.10 e^- $bohr^{-5}$) at this BCP are consistent with a closed-shell H-bonding interaction.[21]

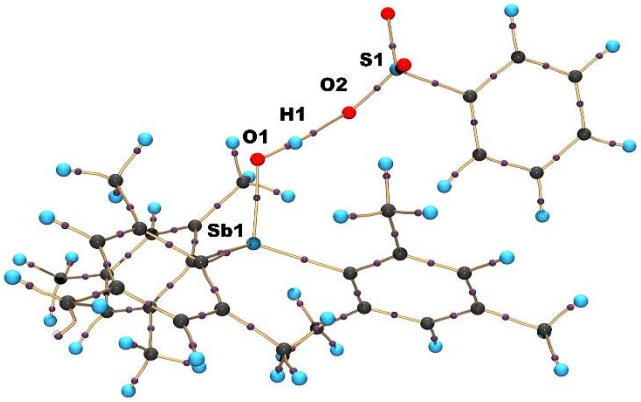

Figure 2. Molecular graph of [Mes_3SbOH][O_3SPh] from the MM charge density. Color code: (3, –1) purple, Sb/S blue, C black, H teal. Bond paths are shown as tan lines. Ring critical points and critical points from crystal packing and intermolecular interactions other than the SbOH···OS H-bond are omitted for clarity.

The difference Fourier synthesis based on the theoretical electron density used in *NoSpherA2* exhibits the same lack of features as the MM difference Fourier map. We note that the HAR electron density agrees with the experimental structure factors to at least the same extent as the refined MM electron density, despite the fact that the former is a purely theoretical value that has not been informed by experiment. This result suggested to us that topological analysis of the electron density used to generate the aspherical form factors for HAR could recover the same information as provided by topological analysis of the MM electron density without the need for complex multipole modelling, which in turn requires neutron-derived (or estimated) H-atom parameters. Conveniently, a by-product of HAR as implemented in *NoSpherA2* is a *.wfn file suitable for topological analysis. We note that this electron density is not a refined, fitted or constrained electron density of the type generated from multipole modelling or X-ray wavefunction refinement;[23-25] it is a purely theoretical quantum-mechanical electron density that

is conveniently available as a byproduct of the HAR process. This theoretical electron density exhibits all of the same molecular critical points as the MM electron density. The similarity in the locations of the critical points is reflected in the agreement of the positions of the BCPs along the bond paths (Figure 3A). The C–H bonds are the notable exception, with the MM BCPs appearing slightly closer to the H atoms.

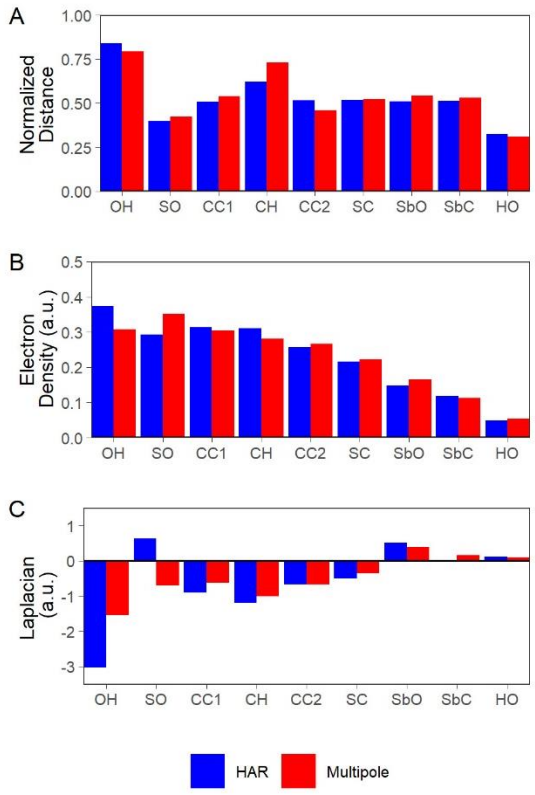

Figure 3. Values of (A) the normalized distances (e.g., from O to H for OH), (B) ρ, and (C) $\nabla^2\rho$ at the BCPs derived from the MM (red) and HAR (blue). For (A) bond lengths are normalized to unit length; values reflect the fraction of the bond length along the bond at which the BCP occurs. CC1 = C_{Ar}–C_{Ar}, CC2 = C_{Ar}–C_{Me}, CH = C_{Me}–H_{Me}. For bond types that arise multiple times, a representative example was selected.

The ρ_b values show minor discrepancies in magnitude, the greatest of which is associated with the polar O–H bond (Figure 3B); the theoretical model based on the HAR geometry returns a greater ρ_b. Analysis of $\nabla^2\rho_b$ (Figure 3C) suggests that the theoretical model based on the HAR geometry also favors local charge concentration in this bonding interaction: the HAR $\nabla^2\rho_b$ value is lower (i.e., more negative) than the MM value. A comparison of MM and X-ray wavefunction refinement of the polar bonds in a panel of amino acids and tripeptides revealed that the MM tends to underestimate $\nabla^2\rho_b$.[25] Nevertheless, both models generally track each other well in the present study. A notable discrepancy is found in the S–O bonds: HAR and MM values of ρ_b differ slightly, but the corresponding values of $\nabla^2\rho_b$ vary greatly in magnitude and sign. This discrepancy is resolved below.

A more nuanced comparison of the theoretical model based on the HAR geometry and multipole models can be achieved using the behavior of ρ and $\nabla^2\rho$ along the length of a bond path or across a plane. The full bond path analyses of ρ (Figure S5) recover the close positioning of the BCPs (Figure 3A) and the large apparent discrepancy noted for the C–H bonds can now be understood as arising from a relatively shallow well in ρ. Comparison of $\nabla^2\rho$ along the bond paths (Figure S6) shows that they exhibit similar local maxima and minima. The overall similarity between the two models can be further appreciated by comparing the similarities in 2D contour plots of ρ (Figure S7) and $\nabla^2\rho$ (Figure S8). We can also appreciate that the disparity between the HAR and MM values of $\nabla^2\rho_b$ for the S–O bond arise simply because the BCP falls in a region where $\nabla^2\rho$ is varying sharply as a function of distance in the vicinity of $\nabla^2\rho_b = 0$ (Figure S6). Analyzing the behavior of ρ and $\nabla^2\rho$ along the entire bond path reveals, however, the similarities in these bonds.

Finally, we note that the collective properties of the theoretical ρ, $\nabla^2\rho$, and ellipticity (ε) along the Sb–O bond path are fully consistent with the earlier trends we reported for an Sb–O single bond in a hydroxystibonium cation (Figure 4).[22] Specifically, the BCP lies approximately halfway along the bond path, $\nabla^2\rho$ features a single O-proximal minimum in the valence region, and ε lacks a distinct maximum near the middle of the bond path but instead rises gradually to an O-proximal maximum. These functions, notably ε, would present differently for a stibine oxide.[22]

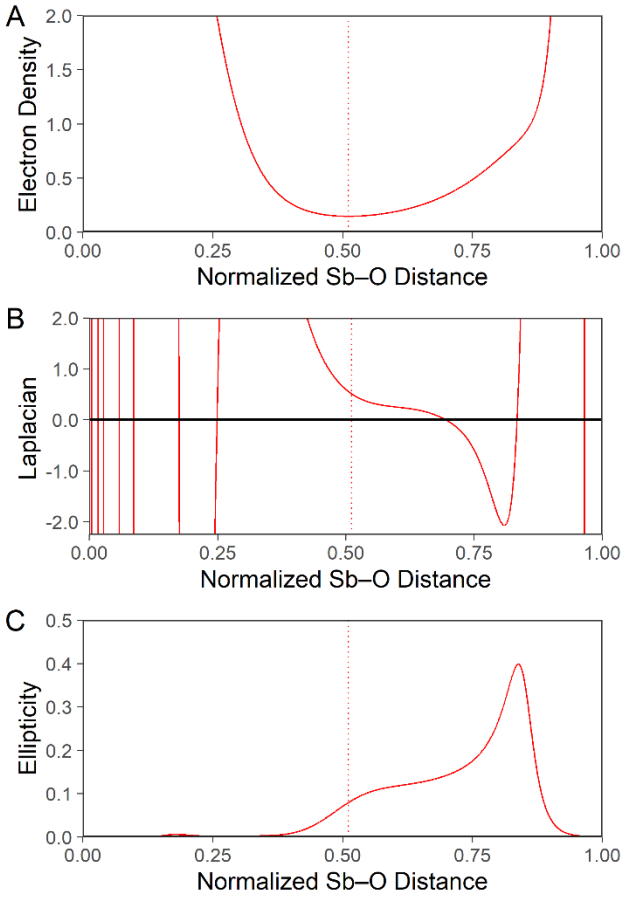

Figure 4. Values of (A) ρ, (B) $\nabla^2\rho$, and (C) ε along the normalized length of the Sb–O bond (Sb at left, O at right) in the theoretical model based on the HAR geometry of $[Mes_3SbOH][O_3SPh]$. Vertical dotted line marks the position of the BCP. All values are in atomic units.

In conclusion, HAR with *NoSpherA2* was performed on [Mes_3SbOH][O_3SPh], a structure featuring a heavy atom, a polar O–H bond, and intramolecular H-bonding. HAR H-atom positions and ADPs agreed exceptionally well with those obtained from neutron diffraction. The theoretical electron density model based on the HAR geometry features a topology that matches that of the experimentally refined MM charge density. This result aligns with an earlier prediction that "…in the future a simple HAR can be used as a reliable, easy, and fast approximation to the experimental electron density in the crystal."[25] HAR also identified a H-atom disorder that could not be diagnosed in the X-ray IAM. The present work demonstrates yet another facet to the utility of the *NoSpherA2* interface, which we anticipate will enable chemists engaged in a range of areas to more deeply interrogate their systems using home-source X-ray data to access information that would typically require national-facility beamlines.

ASSOCIATED CONTENT

Supporting Information.

The following files are available free of charge.

experimental details, refinement details, tabulated values (PDF)

crystallographic data, CCDC 2093680-2093682 (CIF)

AUTHOR INFORMATION

Corresponding Author

*johnstone@ucsc.edu

Author Contributions

The manuscript was written through contributions of all authors. All authors have given approval to the final version of the manuscript.

ACKNOWLEDGMENT

The single-crystal X-ray diffractometer housed in the UCSC X-ray Diffraction Facility was funded by NSF MRI grant 2018501. This research used resources at the Spallation Neutron Source, a DOE Office of Science User Facility operated by the Oak Ridge National Laboratory.

REFERENCES

1. Wenger, J. S.; Johnstone, T. C., Unsupported monomeric stibine oxides (R_3SbO) remain undiscovered. *Chem. Commun.* **2021,** *57*, 3484-3487.

2. Huber, F.; Westhoff, T.; Preut, H., Tris(2,4,6-trimethylphenyl)antimony dihydroxide; synthesis and reaction with sulfonic acids RSO_3H (R = C_6H_5, CF_3). Crystal structure of $[2,4,6\text{-}(CH_3)_3C_6H_2]_3SbO \cdot HO_3SC_6H_5$. *J. Organomet. Chem.* **1987,** *323*, 173-180.

3. Dolomanov, O. V.; Bourhis, L. J.; Gildea, R. J.; Howard, J. A. K.; Puschmann, H., OLEX2: a complete structure solution, refinement and analysis program. *J. Appl. Crystallogr.* **2009,** *42*, 339-341.

4. Kleemiss, F.; Dolomanov, O. V.; Bodensteiner, M.; Peyerimhoff, N.; Midgley, L.; Bourhis, L. J.; Genoni, A.; Malaspina, L. A.; Jayatilaka, D.; Spencer, J. L.; White, F.; Grundkötter-Stock, B.; Steinhauer, S.; Lentz, D.; Puschmann, H.; Grabowsky, S., Accurate crystal structures and chemical properties from NoSpherA2. *Chem. Sci.* **2021,** *12*, 1675-1692.

5. Jayatilaka, D.; Dittrich, B., X-ray structure refinement using aspherical atomic density functions obtained from quantum-mechanical calculations. *Acta Crystallogr. A.* **2008,** *64*, 383-393.

6. Capelli, S. C.; Bürgi, H.-B.; Dittrich, B.; Grabowsky, S.; Jayatilaka, D., Hirshfeld atom refinement. *IUCrJ* **2014,** *1*, 361-379.

7. Woińska, M.; Grabowsky, S.; Dominiak, P. M.; Woźniak, K.; Jayatilaka, D., Hydrogen atoms can be located accurately and precisely by x-ray crystallography. *Sci. Adv.* **2016,** *2*, e1600192.

8. Fugel, M.; Jayatilaka, D.; Hupf, E.; Overgaard, J.; Hathwar, V. R.; Macchi, P.; Turner, M. J.; Howard, J. A. K.; Dolomanov, O. V.; Puschmann, H.; Iversen, B. B.; Bürgi, H.-B.; Grabowsky, S., Probing the accuracy and precision of Hirshfeld atom refinement with HARt interfaced with Olex2. *IUCrJ* **2018,** *5*, 32-44.

9. Wanat, M.; Malinska, M.; Gutmann, M. J.; Cooper, R. I.; Wozniak, K., HAR, TAAM and BODD refinements of model crystal structures using Cu Kα and Mo Kα X-ray diffraction data. *Acta Crystallogr. B.* **2021,** *77*, 41-53.

10. Chodkiewicz, M. L.; Woińska, M.; Woźniak, K., Hirshfeld atom like refinement with alternative electron density partitions. *IUCrJ* **2020,** *7*, 1199-1215.

11. Grabowsky, S.; Genoni, A.; Bürgi, H.-B., Quantum crystallography. *Chem. Sci.* **2017,** *8*, 4159-4176.

12. Genoni, A.; Bučinský, L.; Claiser, N.; Contreras-García, J.; Dittrich, B.; Dominiak, P. M.; Espinosa, E.; Gatti, C.; Giannozzi, P.; Gillet, J. M.; Jayatilaka, D.; Macchi, P.; Madsen, A. Ø.; Massa, L.; Matta, C. F.; Merz, K. M.; Nakashima, P. N. H.; Ott, H.; Ryde, U.; Schwarz, K.; Sierka,

M.; Grabowsky, S., Quantum Crystallography: Current Developments and Future Perspectives. *Chem. - Eur. J.* **2018,** *24*, 10881-10905.

13. Grabowsky, S.; Genoni, A.; Thomas, S. P.; Jayatilaka, D., The Advent of Quantum Crystallography: Form and Structure Factors from Quantum Mechanics for Advanced Structure Refinement and Wavefunction Fitting. Springer International Publishing: 2020; pp 65-144.

14. Genoni, A.; Macchi, P., Quantum Crystallography in the Last Decade: Developments and Outlooks. *Crystals* **2020,** *10*, 473.

15. Jayatilaka, D.; Grimwood, D. J., Tonto: A Fortran Based Object-Oriented System for Quantum Chemistry and Crystallography. In *Computational Science — ICCS 2003*, Sloot, P. M. A.; Abramson, D.; Bogdanov, A. V.; Gorbachev, Y. E.; Dongarra, J. J.; Zomaya, A. Y., Eds. Springer Berlin Heidelberg: Berlin, Heidelberg, 2003; pp 142-151.

16. Allen, F. H.; Bruno, I. J., Bond lengths in organic and metal-organic compounds revisited: X—H bond lengths from neutron diffraction data. *Acta Crystallogr. B.* **2010,** *66*, 380-386.

17. Perdew, J. P.; Ernzerhof, M.; Burke, K., Rationale for mixing exact exchange with density functional approximations. *J. Chem. Phys.* **1996,** *105*, 9982-9985.

18. Perdew, J. P.; Burke, K.; Ernzerhof, M., Generalized Gradient Approximation Made Simple. *Phys. Rev. Lett.* **1996,** *77*, 3865-3868.

19. Pollak, P.; Weigend, F., Segmented Contracted Error-Consistent Basis Sets of Double- and Triple-ζ Valence Quality for One- and Two-Component Relativistic All-Electron Calculations. *J. Chem. Theory Comput.* **2017,** *13*, 3696-3705.

20. Merritt, E. A., Comparing anisotropic displacement parameters in protein structures. *Acta Crystallogr. D.* **1999,** *55*, 1997-2004.

21. Bader, R. F. W.; *Atoms in Molecules: A Quantum Theory*. Clarendon Press: 1994.

22. Lindquist-Kleissler, B.; Wenger, J. S.; Johnstone, T. C., Analysis of Oxygen–Pnictogen Bonding with Full Bond Path Topological Analysis of the Electron Density. *Inorg. Chem.* **2021,** *60*, 1846-1856.

23. Grabowsky, S.; Luger, P.; Buschmann, J.; Schneider, T.; Schirmeister, T.; Sobolev, A. N.; Jayatilaka, D., The Significance of Ionic Bonding in Sulfur Dioxide: Bond Orders from X-ray Diffraction Data. *Angew. Chem. Int.* **2012,** *51*, 6776-6779.

24. Jayatilaka, D., Wave Function for Beryllium from X-Ray Diffraction Data. *Phys. Rev. Lett.* **1998,** *80*, 798-801.

25. Woińska, M.; Jayatilaka, D.; Dittrich, B.; Flaig, R.; Luger, P.; Woźniak, K.; Dominiak, P. M.; Grabowsky, S., Validation of X-ray Wavefunction Refinement. *ChemPhysChem* **2017,** *18*, 3334-3351.

SYNOPSIS

Neutron diffraction and multipole-modeled X-ray diffraction confirm that $[Mes_3Sb(OH)][O_3SPh]$ is indeed a hydroxystibonium sulfonate salt. Hirshfeld atom refinement (HAR) affords H-atom parameters consistent with the neutron diffraction values and the theoretical electron density used for HAR exhibits a topology that matches that of the multipole model.

TOC GRAPHIC

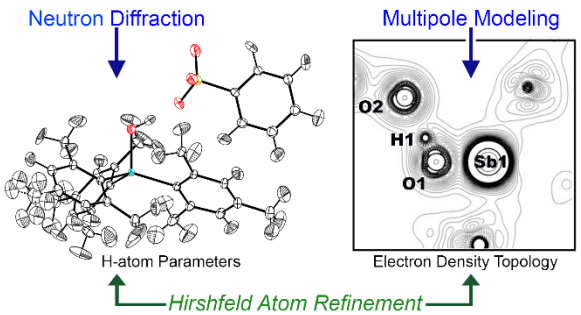

Supporting Information for

H-Atom Assignment and Sb–O Bonding of [Mes_3SbOH][O_3SPh] Confirmed by Neutron Diffraction, Multipole Modeling, and Hirshfeld Atom Refinement

John S. Wenger,[a] Xiaoping Wang,[b] and Timothy C. Johnstone[a]*

[a] Department of Chemistry and Biochemistry, University of California Santa Cruz, Santa Cruz, California 95064, United States.

[b] Neutron Scattering Division, Oak Ridge National Laboratory, Oak Ridge, Tennessee 37831, United States.

* johnstone@ucsc.edu

CONTENTS

Experimental Methods

Neutron Diffraction. [Mes_3SbOH][O_3SPh] was synthesized and crystallized as previously reported.[1] A colorless prism measuring 1.08 × 0.80 × 0.35 mm^3 was attached onto a MiTGen loop using perfluorinated grease (Krytox GPL 205) and mounted on the TOPAZ goniometer. The sample was cooled to 100 K under an cold nitrogen stream and irradiated using TOPAZ at the Spallation Neutron Source (SNS) of Oak Ridge National Laboratory.[2] Data were collected using 17 crystal orientations optimized with CrystalPlan[3] software for better than 99% coverage of symmetry-equivalent reflections of the orthorhombic cell. Each orientation was measured for approximately 5 h with 25 C of proton charge at an SNS beam power of 1.4 MW. The integrated raw Bragg intensities were obtained using 3-D ellipsoidal Q-space integration in accordance with previously reported methods.[4] The reflections could be observed out to a resolution of 0.79 Å. Data reduction, including neutron TOF spectrum, Lorentz, and detector efficiency corrections, was carried out with the ANVRED3 program.[5] Gaussian numerical absorption correction was applied with $\mu = 0.13489 + 0.10068\lambda$ mm^{-1}. The reduced data were saved in SHELX HKLF2 format, in which the wavelength is recorded separately for each reflection, and data were not merged. Our previously-reported X-ray IAM was used as the starting point for refinement with SHELXL.[6] The positions and ADPs of the H atoms were allowed to refine freely while non-H-atom positions and ADPs were constrained to the IAM values. The neutron data revealed the presence of disorder in one of the methyl groups. The disordered methyl group was split into two parts related by rotational symmetry and refined anisotropically while employing rigid bond and similarity restraints. Refinement parameters are collected in Table S1.

X-ray Diffraction: Independent Atom Model. Previously reported X-ray diffraction data for [Mes_3SbOH][O_3SPh] were used.[1] The experimental details and independent atom model (IAM) refinement procedure are repeated here for convenience. A crystal was selected under a microscope, loaded onto a nylon fiber loop using Paratone-N, and mounted onto a Rigaku XtaLAB Synergy-S single crystal diffractometer. The crystal was cooled to 100 K under a stream of nitrogen. Diffraction of Mo Kα radiation from a PhotonJet-S microfocus source was detected using a HyPix6000HE hybrid photon counting detector. Screening, indexing, data collection, and data processing were performed with CrysAlis^{Pro}.[7] The structures were solved using SHELXT and refined using SHELXL following established strategies.[6,8-9] All non-H atoms were refined anisotropically. Carbon-bound H atoms were placed at calculated positions and refined with a riding model and coupled isotropic displacement parameters (1.2 × U_{eq} for aryl groups and 1.5 × U_{eq} for methyl groups). The oxygen-bound H atom was located in the difference Fourier synthesis; its positional parameters were refined semi-freely and its isotropic displacement parameter was set equal to 1.5 × U_{eq} of the oxygen atom. Refinement parameters are collected in Table S1.

X-ray Diffraction: Hirshfeld Atom Refinement. Our previously reported IAM of [Mes_3SbOH][O_3SPh] was refined using the *NoSpherA2* implementation of HAR in *Olex2* with the *olex2.refine* engine.[10] The quantum chemistry calculations were performed by ORCA (version 4.2.1).[11-12] A wavefunction was calculated with tight SCF convergence criteria using the PBE0 hybrid functional and the x2c-TZVPP all-electron relativistically contracted basis set.[13-16] The effects of relativity were introduced using the second-order Douglass-Kroll-Hess formalism.[17] The

ADPs and positions of all atoms, including H atoms, were freely refined using the aspherical atomic form factors obtained from Hirshfeld stockholder partitioning of the computed wavefunction.[18] The newly refined atomic coordinates were used as the input for a new density functional theory (DFT) calculation, from which new aspherical form factors were obtained. This procedure was iterated until it had converged. The ADPs of the H atoms produce well-formed thermal ellipsoids with the exception of a single methyl group, where the H-atom ellipsoids are elongated and suggestive of rotational disorder. The HAR was repeated under the same conditions from the IAM after splitting the disordered methyl group into two parts related by rotational symmetry. The disordered H atoms were non-positive definite after refinement. Rigid bond and similarity restraints were applied to all disordered H atoms, and the minor component was refined isotropically without recalculating the wavefunctions and tabulated aspherical atomic form factors. Refinement parameters are collected in Table S1. H-atom ADPs from the neutron (Table S5) and HAR (Table S6) structures were compared quantitatively with correlation coefficients (Figure S1 and Table S7).[19]

X-ray Diffraction: Multipole Refinement. The full MM refinement strategy is described in Table S9. The atomic coordinates and thermal parameters from the X-ray IAM were used as a starting point for the multipole refinement, which was carried out under the Hansen-Coppens formalism[20] using the full-matrix-least-squares refinement program XDLSM within the *XD2016* suite. Form factors were derived from the STO wavefunctions of the Volkov-Macchi-ZORA databank within the *XD2016* suite. An initial site symmetry-restricted multipolar expansion was performed with the C, O, S, and Sb functions truncated at an octupolar level, the Sb–O*H* atom at a quadrupolar level, and the C*H* atoms at a dipolar level. Chemical similarity constraints were employed for the initial stages of refinement. The non-H-atom atomic coordinates and thermal parameters were allowed to refine again. At this stage, the κ parameters for non-H atoms (one for each element type) were then allowed to refine while κ and κ' for H atoms were set to 1.13 and 1.18, respectively. The H-atom coordinates were allowed to refine, while being reset to the neutron model bond lengths at each stage of refinement. The neutron model H-atom thermal parameters were then added to the model but not refined. A subsequent multipolar expansion was performed with all non-H atoms truncated at the hexadecapolar level and all H atoms truncated at the quadrupolar level. The number of κ parameters was allowed to increase (one for each chemically equivalent atom type) and the H-atom κ parameters were allowed to refine. Site symmetry and chemical similarity constraints were systematically relaxed until they were only applied to H atoms. Inspection of the difference Fourier synthesis revealed no clear peaks corresponding to unmodelled valence electron density (Figure S3). The final multipole model (MM) featured satisfactory residual factors (Table S1).

Topological Analysis. The electron density and Laplacian of the MM were calculated using the *XDPROP* program within the *XD2016* suite. Topological analyses were performed with *Multiwfn*[21] using the cube files for the MM and the wavefunction file from *NoSpherA2* HAR. The electron density and Laplacian values along interatomic vectors and 2D planes were calculated using *Multiwfn.* The values of these real-space functions along the chosen interatomic lines were visualized and the bond critical points were extracted using R (version 4.0.2) through RStudio

(version 1.3.1073). The following R packages were used for analysis and visualization: ggplot2, tidyverse, gridExtra, ggtext, and grid.

References

1. Wenger, J. S.; Johnstone, T. C., Unsupported monomeric stibine oxides (R_3SbO) remain undiscovered. *Chem. Commun.* **2021,** *57*, 3484-3487.
2. Coates, L.; Cao, H.; Chakoumakos, B.; Frontzek, M.; Hoffmann, C.; Kovalevsky, A.; Liu, Y.; Meilleur, F.; dos Santos, A.; Myles, D.; Wang, X.; Ye, F., A suite-level review of the neutron single-crystal diffraction instruments at Oak Ridge National Laboratory. *Rev. Sci. Instrum.* **2018,** *89*, 092802.
3. Zikovsky, J.; Peterson, P.; Wang, X.; Frost, M.; Hoffmann, C., CrystalPlan: An experiment-planning tool for crystallography. *J. Appl. Crystallogr.* **2011,** *44*, 418-423.
4. Schultz, A. J.; Jorgensen, M.; Wang, X.; Mikkelson, R.; Mikkelson, D.; Lynch, V.; Peterson, P.; Green, M.; Hoffmann, C., Integration of neutron time-of-flight single-crystal Bragg peaks in reciprocal space. *J. Appl. Crystallogr.* **2014,** *47*, 915-921.
5. Schultz, A. J.; Srinivasan, K.; Teller, R. G.; Williams, J. M.; Lukehart, C. M., Single-Crystal Time-of-Flight Neutron-Diffraction Structure of Hydrogen *cis*-Diacetyltetracarbonylrhenate, [*cis*-$(OC)_4Re(CH_3CO)_2$]H - a Metallaacetylacetone Molecule. *J. Am. Chem. Soc.* **1984,** *106*, 999-1003.
6. Sheldrick, G. M., Crystal structure refinement withSHELXL. *Acta Crystallogr. C. Struct. Chem.* **2015,** *71*, 3-8.
7. Rigaku Oxford Diffraction, *CrysAlis^{Pro}* **2020**.
8. Sheldrick, G. M., SHELXT– Integrated space-group and crystal-structure determination. *Acta Crystallogr. A.* **2015,** *71*, 3-8.
9. Müller, P., Practical suggestions for better crystal structures. *Crystallogr. Rev.* **2009,** *15*, 57-83.
10. Kleemiss, F.; Dolomanov, O. V.; Bodensteiner, M.; Peyerimhoff, N.; Midgley, L.; Bourhis, L. J.; Genoni, A.; Malaspina, L. A.; Jayatilaka, D.; Spencer, J. L.; White, F.; Grundkötter-Stock, B.; Steinhauer, S.; Lentz, D.; Puschmann, H.; Grabowsky, S., Accurate crystal structures and chemical properties from NoSpherA2. *Chem. Sci.* **2021,** *12*, 1675-1692.
11. Neese, F., The ORCA program package. *Wiley Interdiscip. Rev.-Comput. Mol. Sci* **2012,** *2*, 73-78.
12. Neese, F., WIREs Comput. Mol. Sci. **2012**, *2*, 73–78; b) F. Neese. *WIREs Comput. Mol. Sci* **2018,** *8*, e1327.
13. Weigend, F.; Ahlrichs, R., Balanced basis sets of split valence, triple zeta valence and quadruple zeta valence quality for H to Rn: Design and assessment of accuracy. *Phys. Chem. Chem. Phys.* **2005,** *7*, 3297-3305.
14. Perdew, J. P.; Ernzerhof, M.; Burke, K., Rationale for mixing exact exchange with density functional approximations. *J. Chem. Phys.* **1996,** *105*, 9982-9985.
15. Perdew, J. P.; Burke, K.; Ernzerhof, M., Generalized Gradient Approximation Made Simple. *Phys. Rev. Lett.* **1996,** *77*, 3865-3868.
16. Pollak, P.; Weigend, F., Segmented Contracted Error-Consistent Basis Sets of Double- and Triple-ζ Valence Quality for One- and Two-Component Relativistic All-Electron Calculations. *J. Chem. Theory Comput.* **2017,** *13*, 3696-3705.

17. Wolf, A.; Reiher, M.; Hess, B. A., The generalized Douglas–Kroll transformation. *J. Chem. Phys.* **2002,** *117*, 9215-9226.
18. Hirshfeld, F. L., Bonded-atom fragments for describing molecular charge densities. *Theor. Chim. Acta* **1977,** *44*, 129-138.
19. Merritt, E. A., Comparing anisotropic displacement parameters in protein structures. *Acta Crystallogr. D.* **1999,** *55*, 1997-2004.
20. Hansen, N. K.; Coppens, P., Testing aspherical atom refinements on small-molecule data sets. *Acta Crystallogr. A.* **1978,** *34*, 909-921.
21. Lu, T.; Chen, F., Multiwfn: A multifunctional wavefunction analyzer. *J. Comput. Chem.* **2012,** *33*, 580-592.
22. Allen, F. H.; Bruno, I. J., Bond lengths in organic and metal-organic compounds revisited: X—H bond lengths from neutron diffraction data. *Acta Crystallogr. B.* **2010,** *66*, 380-386.
23. Münch, A.; Knauer, L.; Ott, H.; Sindlinger, C.; Herbst-Irmer, R.; Strohmann, C.; Stalke, D., Insight into the Bonding and Aggregation of Alkyllithiums by Experimental Charge Density Studies and Energy Decomposition Analyses. *J. Am. Chem. Soc.* **2020,** *142*, 15897-15906.

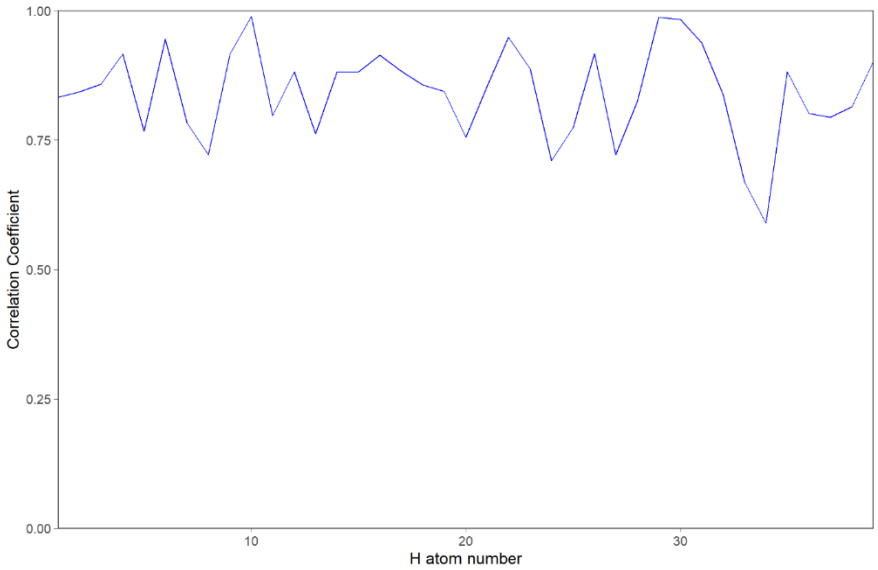

Figure S1. Correlation coefficients between ADPs of H atoms in the neutron diffraction model and the HAR model.

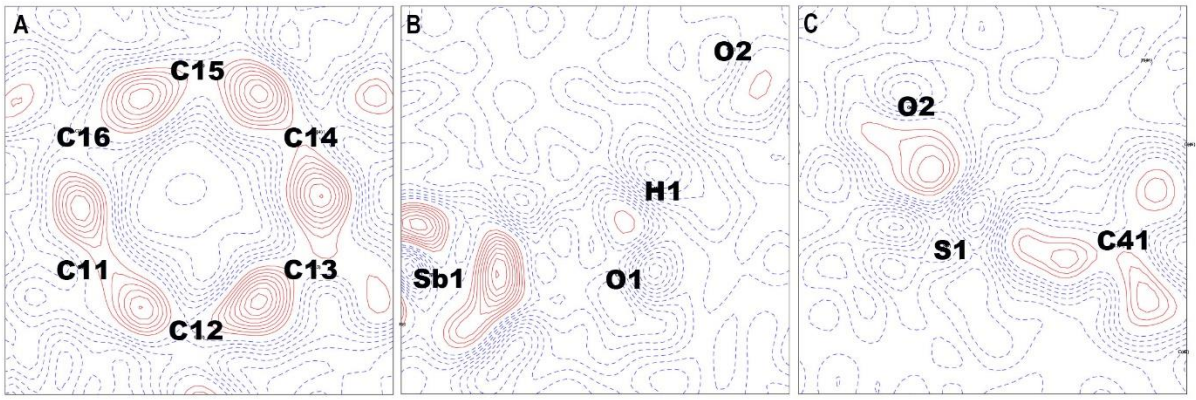

Figure S2. 2D contour plots of the IAM difference Fourier synthesis ($F_o - F_c$) of [Mes_3SbOH][O_3SPh] in the planes defined by (A) C11, C13, and C25, (B) Sb1, O1, and O2, and (C) S1, O2, and C41. Positive contours are shown as red solid lines. Negative contours are shown as blue dashed lines. Contours are drawn at intervals of 0.05 e^- $Å^{-3}$.

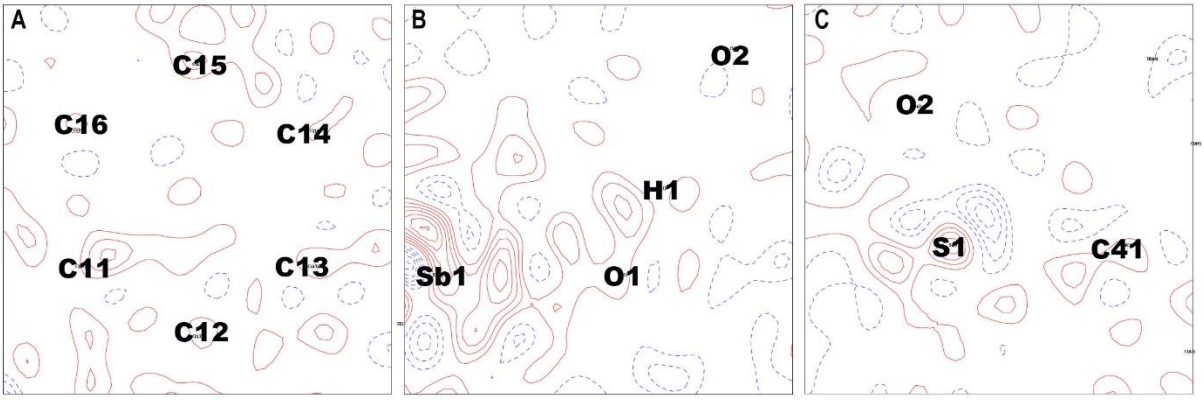

Figure S3. 2D contour plots of the MM difference Fourier synthesis ($F_o - F_c$) of [Mes_3SbOH][O_3SPh] in the planes defined by (A) C11, C13, and C15, (B) Sb1, O1, and O2, and (C) S1, O2, and C41. Positive contours are shown as red solid lines. Negative contours are shown as blue dashed lines. Contours are drawn at intervals of 0.05 e^- $Å^{-3}$.

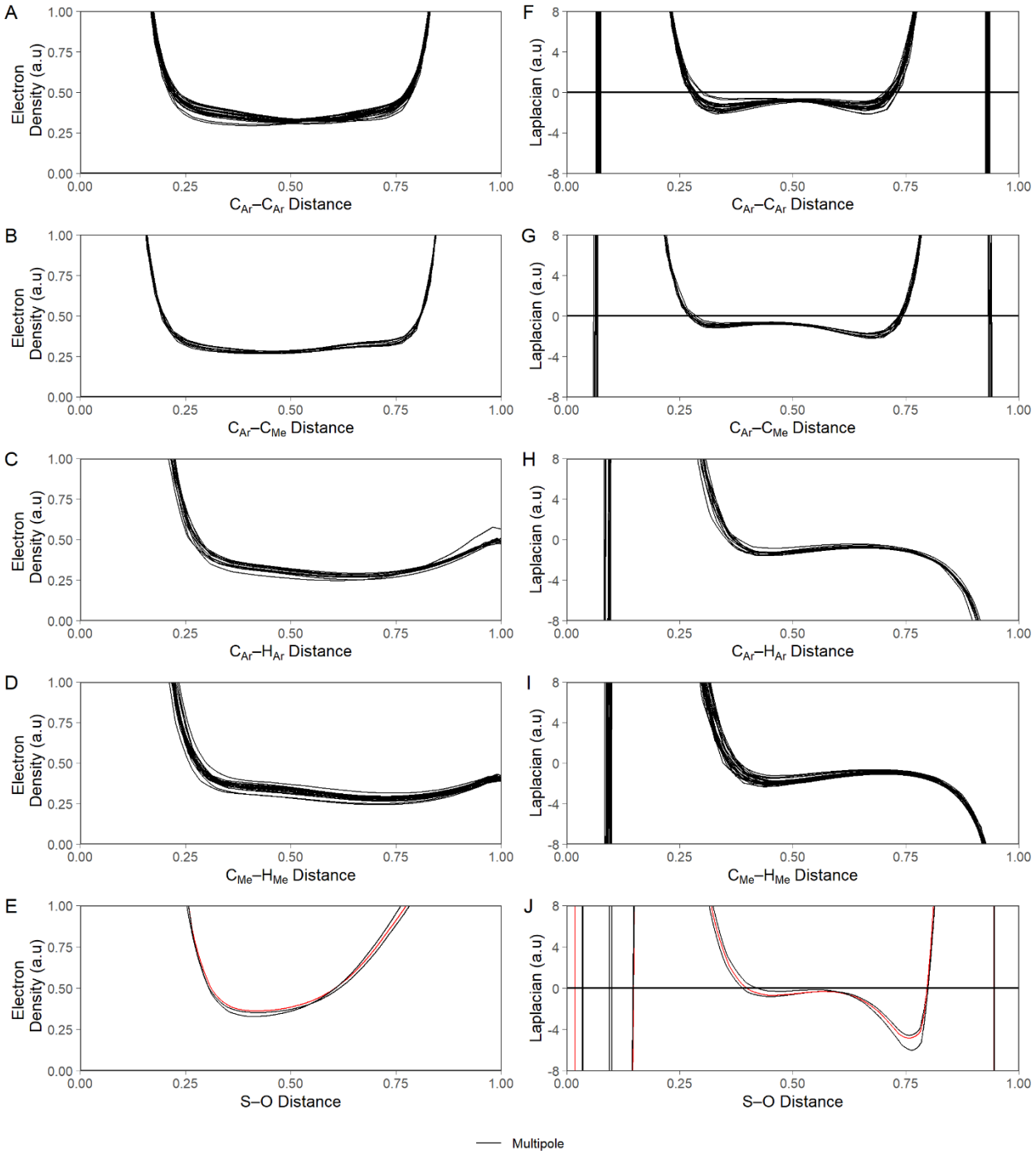

Figure S4. Evaluation of ρ for (A) aryl C–C bonds, (B) methyl C–C bonds, (C) aryl C–H bonds, (D) methyl C–H bonds, and (E) S–O bonds derived from the MM. Evaluation of $\nabla^2\rho$ for (F) aryl C–C bonds, (G) methyl C–C bonds, (H) aryl C–H bonds, (I) methyl C–H bonds, and (J) S–O bonds derived from the MM. Real space functions corresponding to the hydrogen bonding oxygen are shown in red.

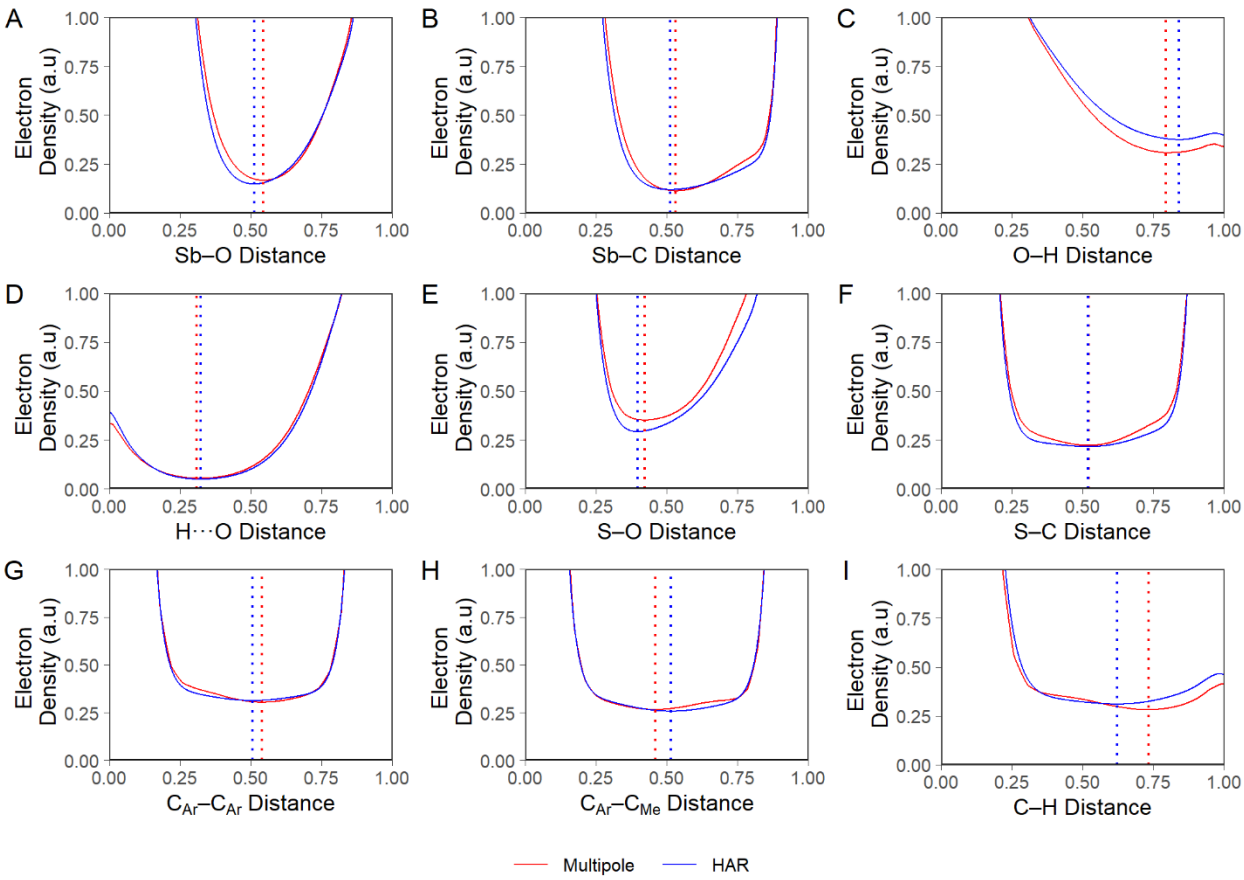

Figure S5. Evaluation of ρ derived from the MM (red) and HAR (blue) along representative interatomic bond paths. Dashed vertical lines represent the bond critical point. Distances are normalized.

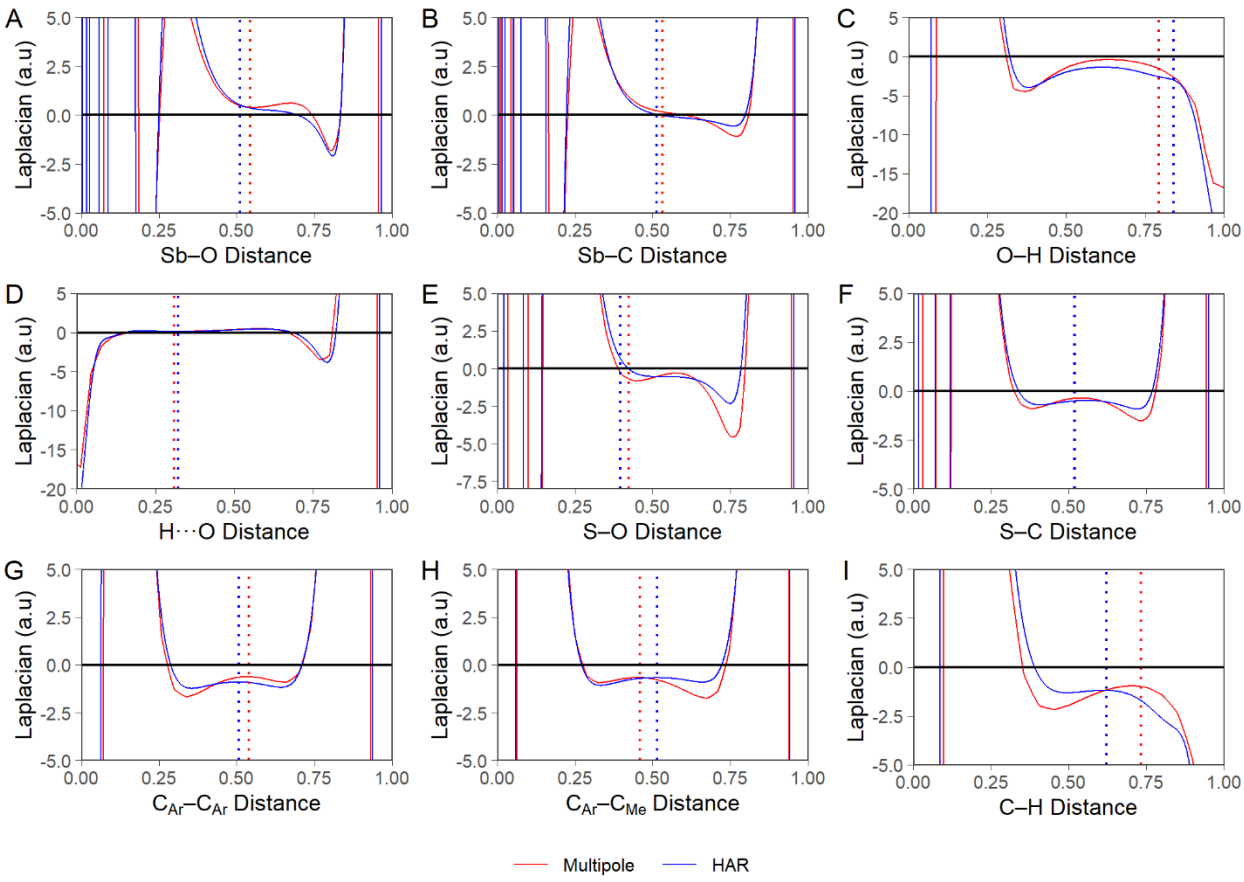

Figure S6. Evaluation of $\nabla^2\rho$ derived from the MM (red) and HAR (blue) along representative interatomic bond paths. Dashed vertical lines represent the bond critical point. Distances are normalized.

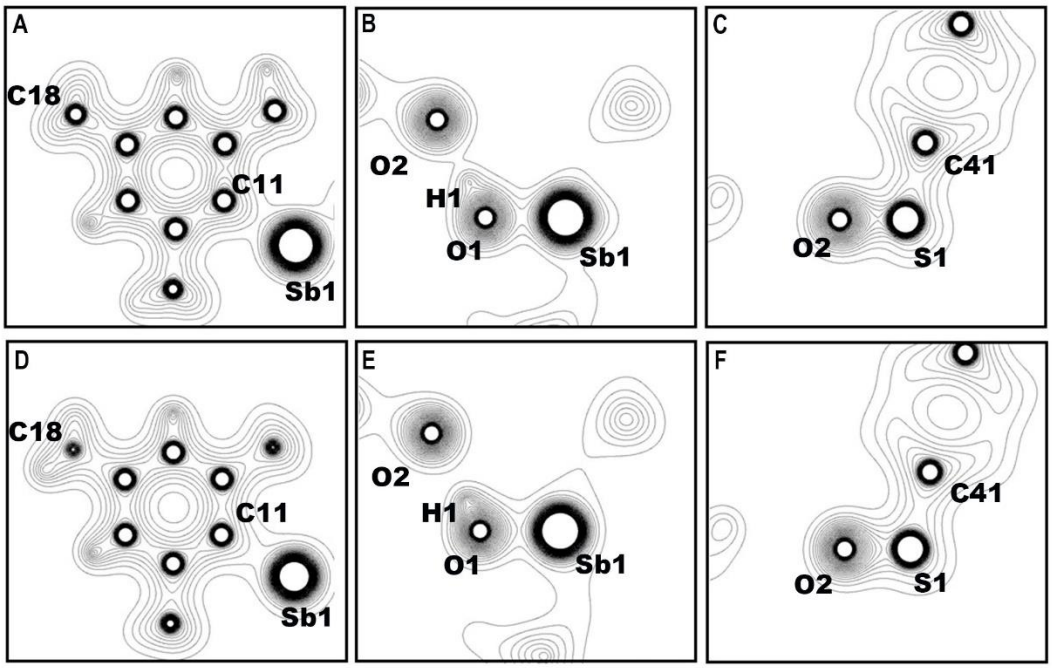

Figure S7. Contour plots of ρ depicting planes defined by the (A, D) C11, C13, and C15 atoms, (B, E) Sb1, O1, and O2 atoms, and (C, F) S1, O2, and C41 atoms derived from the (A-C) MM and (D-F) HAR model. Atom positions are labelled by element symbols. Contours are drawn at intervals of 0.05 e^{-} $Å^{-3}$.

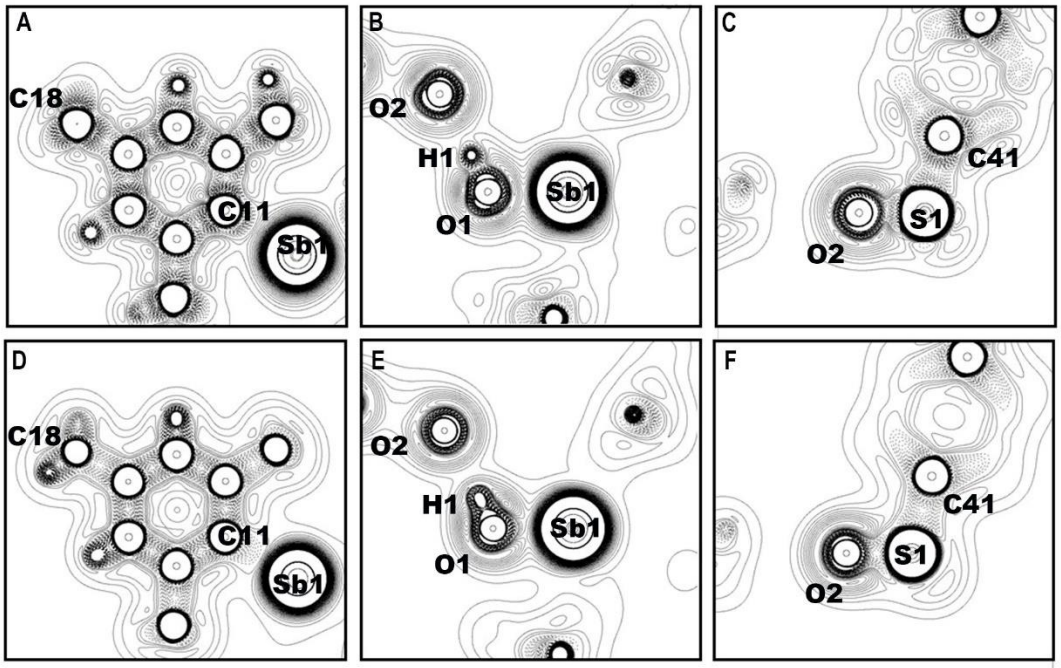

Figure S8. Contour plots of $\nabla^2\rho$ depicting planes defined by the (A, D) C11, C13, and C15 atoms, (B, E) Sb1, O1, and O2 atoms, and (C, F) S1, O2, and C41 atoms derived from the (A-C) MM and (D-F) HAR model. Atom positions are labelled by element symbols. Positive contours are shown as solid lines. Negative contours are shown as dashed lines. Contours are drawn at intervals of 0.05 e^{-} $Å^{-5}$.

Table S1. Crystallographic details for different refinement methods of [Mes_3SbOH][O_3SPh].[a]

	X-ray IAM	**Neutron**	**X-ray HAR**	**X-ray Multipole**
Wavelength (Å)	0.71073	0.41-3.50	0.71073	0.71073
Crystal size (mm^3)	0.19×0.14×0.07	1.05×0.8×0.35	0.19×0.14×0.07	0.19×0.14×0.07
θ range (°)	1.967 to 38.084	7.36 to 78.50	1.97 to 38.08	1.97 to 38.08
Resolution (Å)	0.58	0.79	0.58	0.58
Total reflections	129747	10216	129747	129747
Unique reflections	15556	1941	15556	13013 [c]
Parameters	383	350	703	1472
Completeness (%)	100	N/A[b]	100	100
R_{int}	0.0251	0.1235	0.0251	0.0251
R_1 (I > 2σ)	0.0209	0.0685	0.0157	0.0144 [d]
R_1 (all data)	0.0268	0.0694	0.0216	0.0246
wR_2 (all data)	0.0590	0.1552	0.0372	0.0272
Goodness of fit, *S*	1.028	1.235	1.0317	1.873
Max Peak [e]	1.206	1.600	1.329	0.858
Min Hole [e]	–0.344	–0.871	–0.344	–0.662

[a] Empirical formula: $C_{33}H_{39}O_4SSb$; formula weight: 653.45; temperature: 100(2) K; crystal system: orthorhombic; space group: *Pbca*; *a* 16.62251(11) Å; *b* 16.92326(15) Å; *c* 21.21101(15) Å; volume 5966.81(8) $Å^3$; *Z* 8; ρ_{calc} 1.455 Mg/m^3.

[b] Neutron data were collected with better than 99% coverage for the hydrogenated single crystal sample. Hydrogen is a negative scatterer for neutrons. The completeness appeared low due to the high hydrogen contents (50% atomic hydrogen) in [Mes_3SbOH][O_3SPh], not all peaks had enough neutron counts to be considered as observed.

[c] Reflections with $I < 0$, $I > 1\times10^{10}$, $I/\sigma < 3$, or $I/\sigma > 1\times10^{10}$ were excluded from the refinement but the full 15556 reflections were included in the structure factor calculation.

[d] R_1 (I > 3σ)

[e] For X-ray models, these entries have units of (e^- $Å^{-3}$), and for the neutron model, these entries have units of (*fm* $Å^{-3}$).

Table S2. Hydrogen bond lengths (Å) found from neutron diffraction data and HAR crystal structures.

	Neutron	**HAR**
O(1)-H(1)	0.979(15)	0.99(1)
C(13)-H(13)	1.097(15)	1.10(1)
C(15)-H(15)	1.090(16)	1.09(1)
C(17)-H(17A)	1.08(2)	1.09(1)
C(17)-H(17B)	1.03(2)	1.13(1)
C(17)-H(17C)	1.04(2)	1.07(1)
C(18)-H(18A)	1.09(2)	1.08(1)
C(18)-H(18B)	1.07(2)	1.07(1)
C(18)-H(18C)	1.07(2)	1.12(1)
C(19)-H(19A)	1.09(2)	1.10(1)
C(19)-H(19B)	1.076(18)	1.08(1)
C(19)-H(19C)	1.090(18)	1.11(1)
C(23)-H(23)	1.061(17)	1.095(9)

C(25)-H(25)	1.130(15)	1.089(9)
C(27)-H(27A)	1.07(2)	1.09(1)
C(27)-H(27B)	1.058(19)	1.09(1)
C(27)-H(27C)	1.051(19)	1.09(1)
C(28)-H(28A)	1.11(2)	1.09(1)
C(28)-H(28B)	1.02(2)	1.09(1)
C(28)-H(28C)	1.053(19)	1.10(1)
C(29)-H(29A)	1.077(19)	1.10(1)
C(29)-H(29B)	1.075(16)	1.10(1)
C(29)-H(29C)	1.087(18)	1.08(1)
C(33)-H(33)	1.080(16)	1.104(9)
C(35)-H(35)	1.073(16)	1.11(1)
C(37)-H(37A)	1.084(19)	1.07(1)
C(37)-H(37B)	1.077(15)	1.11(1)
C(37)-H(37C)	1.08(2)	1.08(1)
C(38)-H(38A)	1.13(5)	1.14(3)
C(38)-H(38B)	1.16(5)	1.14(4)
C(38)-H(38C)	0.99(5)	1.04(1)
C(38)-H(38D)	1.12(4)	1.13(2)
C(38)-H(38E)	0.97(4)	1.07(2)
C(38)-H(38F)	1.11(4)	1.13(2)
C(39)-H(39A)	1.07(2)	1.04(1)
C(39)-H(39B)	1.032(18)	1.05(1)
C(39)-H(39C)	1.07(2)	1.04(1)
C(42)-H(42)	1.095(18)	1.11(1)
C(43)-H(43)	1.083(18)	1.12(1)
C(44)-H(44)	1.088(17)	1.11(1)
C(45)-H(45)	1.058(19)	1.12(1)
C(46)-H(46)	1.062(17)	1.08(1)

Table S3. Literature values for averaged bond lengths found from neutron diffraction data.[22]

Bond	**Value**	**σ**
Z—Csp^3—H_3	1.077	0.026
C(ar)—H	1.083	0.017
Z—O—H	0.983	0.025
C(any)—O—H	0.980	0.021

Table S4. U_{eq} ($Å^2 \times 10^3$) of H atoms from neutron diffraction and HAR X-ray crystal structures.

	U_{eq} (Neutron)	**U_{eq} (HAR)**
H(1)	28(4)	48(4)
H(13)	40(4)	52(3)
H(15)	34(4)	40(3)
H(17A)	82(8)	59(3)
H(17B)	62(6)	70(4)
H(17C)	60(6)	81(5)
H(18A)	74(7)	73(5)
H(18B)	69(7)	81(5)
H(18C)	62(6)	73(5)
H(19A)	63(6)	47(3)
H(19B)	59(6)	57(4)
H(19C)	49(5)	60(4)
H(23)	45(5)	51(3)
H(25)	32(4)	42(3)
H(27A)	68(7)	52(3)
H(27B)	62(6)	48(3)
H(27C)	52(5)	46(3)
H(28A)	64(6)	85(5)
H(28B)	66(6)	68(4)
H(28C)	72(7)	76(5)
H(29A)	47(5)	77(5)
H(29B)	50(5)	59(4)
H(29C)	48(5)	64(4)
H(33)	36(4)	51(3)
H(35)	41(4)	58(3)
H(37A)	52(5)	57(4)
H(37B)	49(5)	60(4)
H(37C)	50(5)	58(4)
H(38A)	48(5)	42(7)
H(38B)	47(5)	47(8)
H(38C)	48(5)	25(6)
H(38D)	49(5)	45(2)
H(38E)	51(5)	48(2)
H(38F)	46(5)	46(2)
H(39A)	93(10)	101(6)
H(39B)	69(7)	107(7)
H(39C)	91(10)	73(4)
H(42)	47(5)	49(3)
H(43)	53(5)	58(3)
H(44)	53(5)	58(4)
H(45)	52(5)	62(4)
H(46)	48(5)	55(3)

Table S5. Anisotropic displacement parameters ($Å^2 \times 10^3$) for the neutron model.

	U_{11}	U_{22}	U_{33}	U_{23}	U_{13}	U_{12}
H(1)	31(10)	32(8)	21(7)	0(6)	-10(7)	-9(8)
H(13)	32(10)	23(8)	66(11)	4(8)	18(9)	-9(8)
H(15)	37(11)	35(9)	29(8)	-5(7)	8(8)	-9(8)
H(17A)	140(20)	58(13)	45(11)	1(11)	3(14)	-11(16)
H(17B)	67(15)	15(8)	105(17)	-21(10)	21(13)	-12(9)
H(17C)	60(14)	16(9)	104(17)	5(10)	-10(12)	10(9)
H(18A)	53(14)	120(20)	50(11)	-1(12)	33(11)	-36(13)
H(18B)	61(15)	76(15)	69(14)	9(11)	31(12)	32(13)
H(18C)	51(14)	98(17)	36(9)	16(11)	16(10)	13(12)
H(19A)	53(15)	56(13)	80(14)	-4(11)	16(12)	-25(11)
H(19B)	73(15)	11(8)	91(15)	2(9)	35(13)	0(10)
H(19C)	63(14)	38(11)	47(10)	17(8)	12(10)	-16(9)
H(23)	24(10)	73(13)	38(9)	5(9)	-7(8)	-7(9)
H(25)	23(9)	40(9)	33(8)	10(7)	10(7)	-3(7)
H(27A)	26(12)	110(20)	67(14)	25(13)	10(10)	-4(11)
H(27B)	17(10)	120(20)	51(11)	-2(12)	3(9)	10(11)
H(27C)	36(12)	69(13)	50(11)	-15(10)	10(9)	0(10)
H(28A)	66(15)	77(15)	49(11)	26(11)	-4(12)	-23(13)
H(28B)	47(14)	102(17)	48(11)	19(12)	-10(11)	22(13)
H(28C)	130(20)	34(11)	53(12)	-5(9)	-39(14)	-3(13)
H(29A)	21(10)	59(12)	61(12)	-8(9)	-12(9)	2(9)
H(29B)	26(10)	94(16)	30(8)	-6(10)	5(8)	24(10)
H(29C)	33(11)	53(12)	57(11)	15(10)	-4(9)	9(9)
H(33)	53(12)	21(9)	36(9)	5(7)	-12(8)	9(8)
H(35)	44(12)	16(8)	63(11)	-18(8)	6(10)	5(8)
H(37A)	67(15)	48(11)	41(9)	-23(9)	0(10)	-19(10)
H(37B)	82(16)	48(11)	15(7)	-11(7)	-26(9)	14(10)
H(37C)	45(13)	52(11)	52(11)	-21(9)	-11(9)	14(9)
H(38A)	51(10)	37(10)	57(8)	-2(8)	3(8)	23(9)
H(38B)	51(9)	31(9)	60(10)	8(9)	4(8)	24(8)
H(38C)	51(8)	33(9)	59(8)	-1(8)	0(9)	24(7)
H(38D)	47(9)	42(9)	59(9)	3(9)	4(8)	23(6)
H(38E)	52(9)	40(8)	61(9)	0(8)	0(8)	22(7)
H(38F)	50(10)	31(9)	57(9)	6(7)	4(6)	27(9)
H(39A)	49(15)	190(30)	41(11)	-22(15)	-24(11)	10(17)
H(39B)	97(19)	56(13)	54(11)	-37(10)	-52(13)	29(12)
H(39C)	170(30)	51(13)	56(12)	33(11)	-57(17)	-38(16)
H(42)	58(13)	34(9)	49(10)	19(9)	-11(10)	-29(9)
H(43)	62(14)	61(13)	37(10)	28(10)	-13(10)	-14(11)
H(44)	60(13)	57(12)	41(10)	13(9)	-20(10)	1(10)
H(45)	37(12)	67(13)	52(11)	15(10)	-16(10)	-9(10)
H(46)	54(12)	53(11)	36(9)	6(8)	-2(9)	-30(10)

Table S6. Anisotropic displacement parameters ($Å^2 \times 10^3$) for the HAR model.

	U_{11}	U_{22}	U_{33}	U_{23}	U_{13}	U_{12}
H(1)	58(9)	33(8)	53(9)	-12(6)	5(7)	14(7)
H(13)	57(8)	35(7)	64(8)	-7(5)	-24(6)	-20(5)
H(15)	55(6)	21(5)	45(7)	12(5)	-11(5)	8(5)
H(17A)	43(7)	35(7)	98(10)	-4(7)	-5(7)	13(6)
H(17B)	114(12)	57(10)	40(8)	30(7)	-3(8)	-22(10)
H(17C)	56(8)	51(9)	136(14)	28(9)	-46(9)	-34(7)
H(18A)	54(9)	136(15)	29(7)	-24(7)	13(6)	23(8)
H(18B)	118(12)	57(9)	69(9)	-7(8)	-52(9)	61(9)
H(18C)	55(9)	100(12)	65(9)	7(9)	-27(7)	-36(9)
H(19A)	71(9)	38(7)	31(6)	-5(5)	-13(6)	-4(6)
H(19B)	53(7)	58(9)	61(9)	-3(7)	17(7)	-32(7)
H(19C)	54(7)	32(7)	96(10)	-15(7)	-36(7)	23(6)
H(23)	21(5)	81(9)	52(7)	-16(6)	18(5)	18(5)
H(25)	38(6)	62(8)	24(5)	-9(5)	-6(4)	-9(5)
H(27A)	28(6)	86(9)	41(7)	12(7)	-16(5)	6(6)
H(27B)	42(7)	54(8)	49(7)	-33(6)	5(6)	19(5)
H(27C)	40(6)	42(7)	56(8)	25(6)	13(6)	-9(5)
H(28A)	139(14)	71(11)	46(8)	32(8)	39(9)	-4(10)
H(28B)	60(9)	98(12)	46(8)	-37(7)	-1(6)	-24(9)
H(28C)	44(7)	136(15)	48(8)	-26(8)	9(6)	46(9)
H(29A)	22(6)	166(15)	44(7)	-4(9)	7(5)	16(8)
H(29B)	54(8)	99(11)	24(6)	23(7)	3(6)	2(8)
H(29C)	54(8)	41(7)	98(11)	-37(8)	-21(8)	-9(6)
H(33)	65(7)	63(8)	25(5)	-7(5)	30(5)	5(6)
H(35)	78(9)	34(6)	60(8)	27(6)	21(7)	18(6)
H(37A)	47(7)	62(8)	62(8)	28(7)	-1(6)	36(7)
H(37B)	85(11)	39(8)	57(9)	4(6)	-2(7)	-31(7)
H(37C)	95(10)	54(8)	24(6)	0(6)	25(6)	21(7)
H(38D)	48(4)	36(5)	50(1)	-1(1)	13(1)	12(2)
H(38E)	48(2)	42(5)	53(2)	1(2)	10(1)	14(1)
H(38F)	50(4)	30(3)	57(3)	1(1)	14(1)	13(2)
H(39A)	50(9)	200(20)	49(9)	23(11)	23(7)	4(11)
H(39B)	210(20)	33(8)	79(12)	-35(8)	78(14)	-13(10)
H(39C)	100(11)	77(10)	42(8)	33(7)	27(8)	42(9)
H(42)	41(7)	54(8)	53(8)	-13(6)	16(6)	-29(5)
H(43)	79(9)	42(7)	54(8)	-23(6)	8(6)	-28(7)
H(44)	72(9)	69(10)	33(7)	-22(6)	27(6)	-7(8)
H(45)	45(7)	69(9)	72(9)	0(7)	24(6)	-39(7)
H(46)	71(8)	36(7)	56(8)	-24(6)	13(6)	-21(6)

Table S7. Correlation coefficients (cc) of H-atom ADPs.

	cc
H(1)	0.832696
H(13)	0.843385
H(15)	0.857652
H(17A)	0.916581
H(17B)	0.766857
H(17C)	0.945588
H(18A)	0.78299
H(18B)	0.721625
H(18C)	0.916156
H(19A)	0.988597
H(19B)	0.796888
H(19C)	0.881696
H(23)	0.761786
H(25)	0.881206
H(27A)	0.882148
H(27B)	0.913866
H(27C)	0.882691
H(28A)	0.85669
H(28B)	0.844364
H(28C)	0.755422
H(29A)	0.854291
H(29B)	0.948834
H(29C)	0.888005
H(33)	0.709793
H(35)	0.774052
H(37A)	0.916926
H(37B)	0.721733
H(37C)	0.825541
H(38D)	0.987215
H(38E)	0.982857
H(38F)	0.938197
H(39A)	0.838086
H(39B)	0.668517
H(39C)	0.588946
H(42)	0.882288
H(43)	0.801182
H(44)	0.794034
H(45)	0.814204
H(46)	0.901416

Table S8. Average values of ρ_b and $\nabla^2\rho_b$ derived from the MM with standard deviations provided for bond types occurring more than twice.

Bond Type	ρ_b (e^- bohr^{-3})	$\nabla^2\rho_b$ (e^- bohr^{-5})
C_{Ar}–C_{Ar}	0.32 ± 0.01	–0.79 ± 0.09
C_{Ar}–C_{Me}	0.27 ± 0.006	–0.71 ± 0.08
C_{Ar}–H	0.27 ± 0.014	–0.71 ± 0.11
C_{Me}–H	0.28 ± 0.015	–0.96 ± 0.13
S–O	0.35 ± 0.02	–0.30 ± 0.33
Sb–C	0.10 ± 0.01	0.19 ± 0.06
Sb–O	0.17	0.49
S–C	0.22	–0.37
SbO–H	0.31	–1.54
SbOH···OS	0.053	0.10

Table S9. Multipole modeling refinement strategy[a]

Step	Parameter	#p	d/p	$R_1(F)$	$R_1(F^2)$	R_1(all)	GOF
1	IAM	469	27.74	0.0227	0.0350	0.0329	4.1046
2	Heteroatoms: D Q O C11-C39: D Q O C41-C46: D Q O Hatoms: HD H1D H1Q	189	68.84	0.0188	0.0264	0.0290	2.7086
3	Heteroatoms: M D Q O C11-C39: M D Q O C41-C46: M D Q O Hatoms: M HD H1D H1Q	213	61.08	0.0178	0.0250	0.0280	2.4564
4	Heteroatoms: Uij M D Q O C11-C39: Uij M D Q O C41-C46: Uij M D Q O Hatoms: M HD H1D H1Q	447	29.10	0.0176	0.0242	0.0278	2.3686
5	Heteroatoms: XYZ Uij M D Q O C11-C39: XYZ Uij M D Q O C41-C46: XYZ Uij M D Q O Hatoms: M HD H1D H1Q	564	23.07	0.0175	0.0241	0.0277	2.3325
6	Heteroatoms: k XYZ Uij M D Q O C11-C39: k XYZ Uij M D Q O C41-C46: k XYZ Uij M D Q O Hatoms: M HD H1D H1Q	568	22.90	0.0166	0.0221	0.0268	2.2226
7	HXYZ Neutron Values	122	106.65	0.0177	0.0245	0.0280	2.5611
8	HUij added/HXYZ Neutron Values	122	106.65	0.0180	0.0259	0.0282	2.8848
9	Heteroatoms: k XYZ Uij M D Q O C11-C39: k XYZ Uij M D Q O C41-C46: k XYZ Uij M D Q O Hatoms: M HD H1D H1Q	568	22.90	0.0172	0.0237	0.0274	2.3837
10	H	108	120.48	0.0171	0.0235	0.0273	2.3023
11	H k+	120	108.43	0.0172	0.0234	0.0274	2.3047
12	Hk H k+	121	107.5	0.0171	0.0234	0.0273	2.2889
13	Heteroatoms: NOSITESYMM D Q O H	195	66.72	0.0168	0.0218	0.0270	2.2299

	Hatoms: HD HQ						
14	C11-C39: NOSITESYMM	265	49.10	0.0164	0.0210	0.0266	2.1173
15	C41-C46: NOSITESYMM NOCHEMCON	195	66.72	0.0160	0.0206	0.0262	2.0109
16	Heteroatoms: XYZ Uij M D Q O H C11-C39: XYZ Uij M D Q O H C41-C46: XYZ Uij M D Q O H Hatoms: M HD H1D H1Q	616	21.12	0.0153	0.0201	0.0256	1.9588
17	Heteroatoms: NOSITESYMM XYZ Uij M D Q O H C11-C39: NOSITESYMM XYZ Uij M D Q O H C41-C46: XYZ Uij M D Q O H Hatoms: M HD H1D H1Q	880	14.78	0.0152	0.0199	0.0254	1.9458
18	Heteroatoms: XYZ NOSITESYMM Uij M D Q O H C11-C39: XYZ NOCHEMCON NOSITESYMM Uij M D Q O H C41-C46: XYZ Uij M D Q O H Hatoms: HXYZ M HD H1D H1Q	1470	8.851	0.0146	0.0193	0.0249	1.9947
19	Heteroatoms: NOSITESYMM k XYZ Uij M D Q O H C11-C39: NOCHEMCON NOSITESYMM k XYZ Uij M D Q O H C41-C46: k XYZ Uij M D Q O H Hatoms: Hk HXYZ HQ M HD H1D H1Q	1472	8.83	0.0144	0.0181	0.0246	1.8703

Abbreviations: #p: number of parameters; **d/p:** data to parameter ratio; **GOF:** goodness of fit; **IAM:** the independent atom model was refined using XDLSM; **D:** dipoles, **Q:** quadrupoles, **O:** octupoles; **HD:** H-atom dipoles; **H1D:** H1 dipoles; **H1Q:** H1 quadrupoles; **M:** monopoles; **Uij:** anisotropic thermal parameters; **XYZ:** non-H-atom coordinates; **k:** kappa parameters allowed to refine for non-H atoms (1 per element type); **HXYZ Neutron Values:** H-atom coordinates refined and reset to neutron model bond lengths after each stage of refinement; **HUij added:** neutron derived H-atom thermal parameters added but not refined (disordered H atoms left anisotropic); **H:** hexadecapoles; **k+:** Additional kappa parameters allowed to refine based on chemical differences; **Hk:** H atom kappa parameters allowed to refine; **NOSITESYMM:** site symmetry restrictions on multipolar expansion are removed; **NOCHEMCON:** chemical similarity constraints between atoms are removed

[a] Refinement was performed using established strategies.[23]